Journal of
Synchrotron
Radiation

ISSN 0909-0495

Received 12 October 2005
Accepted 15 January 2006

Development of a scanning tunneling microscope for *in situ* experiments with a synchrotron radiation hard-X-ray microbeam

Akira Saito,[a,b,c]* Junpei Maruyama,[a] Ken Manabe,[a] Katsuyuki Kitamoto,[b] Koji Takahashi,[a] Kazuhiro Takami,[a] Makina Yabashi,[d] Yoshihito Tanaka,[b] Daigo Miwa,[b] Masashi Ishii,[d] Yasumasa Takagi,[b] Megumi Akai-Kasaya,[a,c] Shik Shin,[b] Tetsuya Ishikawa,[b] Yuji Kuwahara[a,b,c] and Masakazu Aono[a,c,e]

[a]Department of Material and Life Science, Osaka University, Osaka 565-0871, Japan, [b]RIKEN/SPring-8, Hyogo 679-5148, Japan, [c]Nanoscale Quantum Conductor Array, ICORP(JST), Saitama 332-0012, Japan, [d]JASRI/SPring-8, Hyogo 679-5198, Japan, and [e]Nanomaterials Laboratory, National Institute for Materials Science, Tsukuba 305-0003, Japan.
E-mail: saito@prec.eng.osaka-u.ac.jp

A scanning tunneling microscope dedicated to *in situ* experiments under the irradiation of highly brilliant hard-X-rays of synchrotron radiation has been developed. *In situ* scanning tunneling microscopy (STM) observation was enabled by developing an accurate alignment system in ultrahigh vacuum. Despite the noisy conditions of the synchrotron radiation facility and the radiation load around the probe tip, STM images were successfully obtained at atomic resolution. Tip-current spectra were obtained for Ge nano-islands on a clean Si(111) surface by changing the incident photon energy across the Ge absorption edge. A current modification was detected at the absorption edge with a spatial resolution of the order of 10 nm.

© 2006 International Union of Crystallography
Printed in Great Britain – all rights reserved

Keywords: scanning tunneling microscopy; hard X-ray microbeam; *in situ* experiments; Ge nano-island; Si(111).

1. Introduction

Scanning tunneling microscopy (STM) has enabled the investigation of morphological and electronic structures in real space at atomic resolution. The combination of the atomic resolution of STM with the energy selectivity or time resolution of light-induced effects has provided various pieces of information on surfaces over the past 15 years (Grafström, 2002). On the other hand, the number of research studies combining STM with X-rays has been quite limited even though such research studies have shown various possibilities of realising original and important applications. One of the advantages of X-rays is their ability to excite the core electrons of a specific level by tuning the photon energy to the binding energy. Specific excitation under STM observation is appealing for discriminating different chemical species on a surface, because X-rays can change the local electron density at a valence orbital by exciting core electrons.

Many approaches to obtaining an STM image with spatially resolved chemical information have been attempted, including the use of tunneling spectroscopy (Papanikolaou *et al.*, 2000), work function (Hasegawa *et al.*, 1997), STM image contrast (Schmid *et al.*, 1993), image states (Viernow *et al.*, 1999), light illumination (Takada *et al.*, 2002), light emission (Downes & Welland, 1998), X-ray-excited AFM (Suzuki *et al.*, 2004) and STM (Tsuji *et al.*, 1999; Hasegawa *et al.*, 2000; Matsushima *et al.*, 2004). Although these approaches are quite valuable and applicable, they are limited in spatial resolution or generality for elemental identification. For approaches other than elemental analysis, successful examples have been reported for inelastic tunneling spectroscopy (Stipe *et al.*, 1998) in the analysis of the molecular vibration states, and for capacitance analysis (Ishii, 2002). In the reports on X-ray-excited STM, some examples have been reported using a probe tip for collecting emitted electrons. These approaches, where the tip collects photoexcited electrons emitted from a wide area, result in a decrease in spatial resolution.

In this paper we show a new approach that is not based on the emitted electrons but on the modulation of the tunneling current, providing the possibility of obtaining local information on the nanometer order. A new STM system enabled an *in situ* experiment with highly brilliant X-rays of diameter 10 μm aligned at the observation point of STM in ultrahigh vacuum (UHV) with an accuracy of 1 μm.

2. Experimental system

2.1. Methodological base

The system was installed at beamline BL19LXU (Yabashi *et al.*, 2001) of SPring-8, that provides the most brilliant hard-X-rays of approximately 2×10^{14} photons s^{-1} under monochromated conditions with a beam size of 500 µm (V) × 1000 µm (H) at the sample position. To remove thermal and electrical noise, damage around the STM scanner or sample, and instabilities of the system such as thermal drift caused by high-intensity X-ray irradiation, it is necessary to adjust the incident beam to as small as possible at the STM observation point (Saito *et al.*, 2000). The essential parameter of the incident beam is not total flux but the photon density just in front of the tip end. The experiments were performed under UHV rather than in gas or the atmosphere to prevent unnecessary excitation that produces many electrons as noise. In brief, we need a three-body alignment (invisible microbeam, sample and tip end) in UHV as fast as possible under a limited machine time at the synchrotron radiation facility. The STM controller and scanner were based on a conventional STM system with a UHV chamber having a base pressure of 1.5×10^{-8} Pa (Jeol, Tokyo, Japan). The STM tip was made from tungsten wire (diameter 0.3 mm) by electrochemical etching with NaOH solution.

2.2. Alignment system

The systems for alignment and monitoring are schematically shown in Figs. 1(*a*) and 1(*b*), respectively. An array of six apertures of different sizes was set upstream of the beam path to change the beam size. In order to decrease a serious radiation load and noise derived from the brilliant X-rays, it is not sufficient to decrease the beam size. For this purpose the total reflection condition is effective, because it strictly limits the penetrating depth of the X-rays into the sample. The rotational axis was introduced below the sample to adjust the incidence angle of the X-rays at the sample surface. There are two transfer motions, X_t and Z_t, used to align the rotational center to the sample surface. The Z_b axis is under the θ stage to align the rotational center to the beam path. An active dumper is used to remove external vibration that is easily produced by resonance in the closed hutch at the beamline. The dumper also has the role of controlling the height of the tip with respect to the X-ray beam with an accuracy of 1 µm.

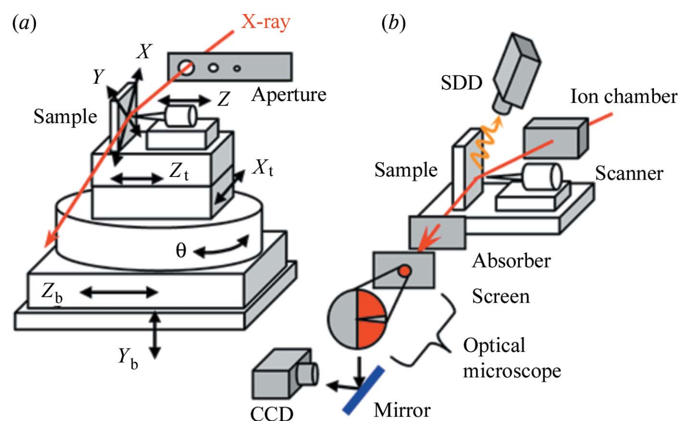

Figure 1
Schematic view of (*a*) the alignment and (*b*) the monitoring system. Under the STM scanner equipped with a standard *XYZ* motion (*a*), an independent four-axis stage is set, whereas the height Y_b is controlled by an air dumper.

2.3. Monitoring system

An ion chamber was set downstream of the aperture to monitor the incident photon count (Fig. 1*b*). To visually confirm the relationship between the sample, tip and X-rays in real time, a silhouette was monitored on a fluorescent screen, which was made of a fluorescent film in crystal to realise a spatial resolution smaller than 1 µm. The screen was placed almost at the sample and tip to avoid losing spatial resolution due to diffraction. The obtained silhouette was magnified by an optical microscope and monitored by a CCD camera through a mirror to prevent radiation damage to the CCD.

Fig. 2 shows the silhouettes obtained with an aperture of diameter 800 µm under low (*a*) and high (*b*) magnifications, and with an aperture of diameter 10 µm under a high magnification (*c*). This system enables the alignment of the X-ray beam of diameter 10 µm to the STM observation point 2 h after the beginning of the experiment with X-rays. An SDD (silicon drift chamber detector, Röntec, Germany) is equipped to detect the fluorescence spectra from the sample and tip. The SDD confirms the existence of adsorbates on the sample and also the alignment between the sample, tip and X-ray beam. The whole system was designed to be operated by remote control from outside the experimental hutch at the beamline because of an interlock system for radiation security.

3. Results and discussions

3.1. STM observation with atomic resolution

First, it is necessary to estimate the influence of damage or noise caused by the synchrotron radiation irradiation on the

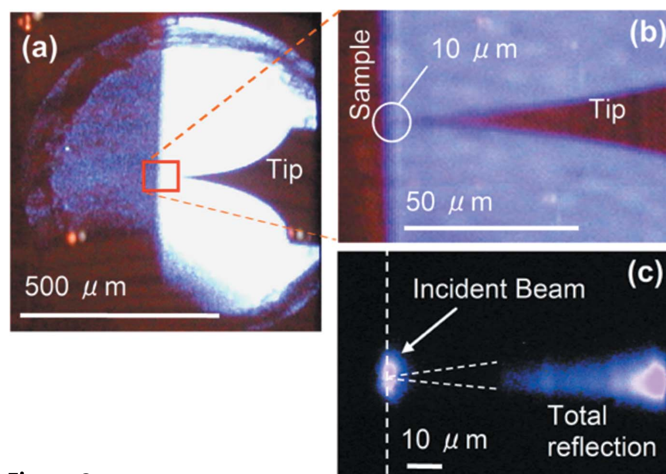

Figure 2
Silhouette images: (*a*) with X-ray beams of diameter 800 µm (magnification ×300) for coarse alignment, (*b*) with higher magnification, (*c*) with X-ray beams of diameter 10 µm. The total reflection is successfully observed, which proves the grazing-incidence condition.

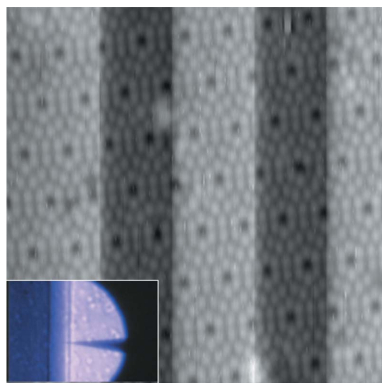

Figure 3
STM image of a clean Si(111) surface with 'on–off' switching of X-ray irradiation. The scan area was 20 nm × 20 nm with a sample bias of +2 V and a tunneling current of 0.3 nA. The inset shows a silhouette in the beam of diameter 200 μm.

STM observation. An X-ray beam of maximum intensity without the aperture will, in fact, break the monitor screen. However, such extensive damage was decreased by limiting the beam size to less than 200 μm diameter. Fig. 3 shows an STM image of a Si(111) 7 × 7 clean surface (n type, 4–7 Ω cm) in the constant-current mode (0.3 nA) with on–off switching of the X-rays, where the inset shows a silhouette in the beam of diameter 200 μm. The energy of the incident beam was 16.5 keV at an incidence angle of 1.5° from the sample surface.

The bright and dark bands in the stripes correspond to the on and off states of the beam, respectively. Since the images were obtained in the constant-current mode, the bright band indicates that the tip is retracted due to the X-ray irradiation. The STM image proves that atomic resolution was successfully obtained in the closed experimental hutch, even under hard X-ray irradiation of the highest brilliance. The origin of this stripe can be ascribed to the electron emission, surface photovoltage or thermal effect. This image modification, which is a serious disrupter of the signal in our case, was effectively removed by use of a 10 μm-diameter aperture and the total reflection condition shown in Fig. 2(*c*).

3.2. Tip-current measurement

One of the most important applications of our system is the analysis of chemical species on the atomic order. In this analysis, emitted electrons that damage spatial resolution are discarded, and the other local parameters with atomic resolution are focused on, *i.e.* the electronic states. For this purpose, it is essential to measure the modulation of the tip current under the tunneling condition, which is caused by excitation at a specific incident energy. Also, the signal detection has a response which is much faster than the tip motion that has been generally used in past reports concerned with the X-ray-excited STM. The incident beam was chopped with a frequency of 3.0 kHz, and the tip current was recorded with integration for 20 ms by a lock-in amplifier (SEIKO, Tokyo, Japan) to obtain a high signal-to-noise ratio. The recorded data are the peak-to-peak values of the tip current under the chopped condition. This approach also has the advantage of guaranteeing accuracy in the determination of the beam-induced current, because the beam-induced current is recorded with respect to a standard base level, *i.e.* the tunneling current under the beam-off condition. The high frequency of the chopper can also effectively reduce the influence of the thermal expansion effect. Actually, the above-mentioned measurement system, which is based on the tip current under the tunneling condition, drastically improved the signal-to-noise ratio and accuracy of data in comparison with the conventional system based on the tip motion (Saito *et al.*, 2006).

3.3. Measurement across the absorption edge

We have demonstrated the elemental analysis using a sample of Ge nano-islands (Fig. 4, right) which was formed after annealing, at 773 K, of a 0.3 monolayer of Ge deposition on a Si(111) 7 × 7 clean surface (Motta *et al.*, 1998; Masuda & Shigeta, 2001). The island formed after Ge deposition is known to be composed of 7 × 7 or 5 × 5 structures. Although the periodicity of the 7 × 7 structure is common with that of the Si(111) clean surface, the islands cannot be formed solely by Si atoms. Since the deposition of many Ge atoms produces a high concentration of the Ge islands, it is natural to consider that the Ge concentration is higher in the islands than in the surrounding area. The difference in composition between the inside and outside of the Ge islands is expected to give a distinction of the signal yield.

The incident beam was focused two-dimensionally to 200 μm (V) × 50 μm (H) using a couple of mirrors to increase the photon density. To reduce the radiation load on the sample, the total reflection condition was maintained with an incident angle of 0.15° from the sample surface, when the

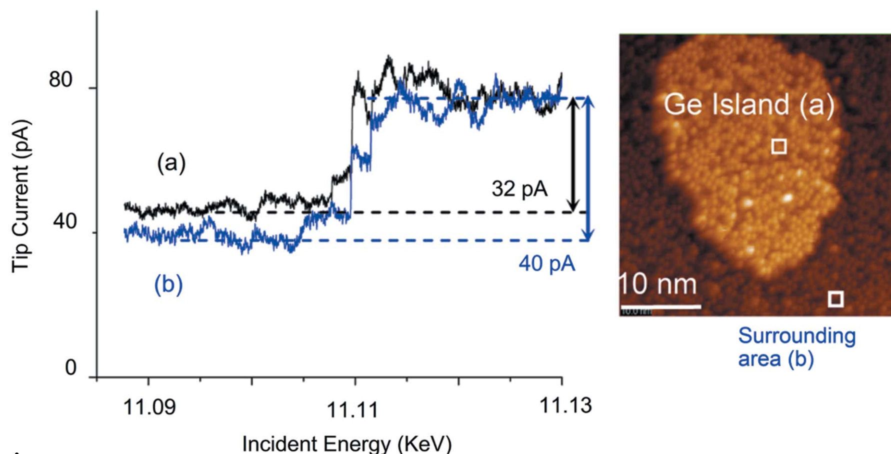

Figure 4
Energy spectra of the tip current (left) on different surface areas under the same tunneling conditions (−2 V, 0.3 nA). Spectra (*a*) and (*b*) were obtained at the areas shown in the right-hand part of the figure (35 nm × 35 nm, −2 V, 0.3 nA).

penetration depth of the X-rays in the substrate was limited to ~3.0 nm. Fig. 4 shows the energy spectra obtained at different areas on the surface, under the common beam condition of 10 μm diameter and the same tunneling conditions. The incident energy was scanned in 1 eV steps and all profiles were normalized by an incident photon count that corresponded to an ion current of 0.33 μA measured by an ion chamber.

Profile (*a*) in Fig. 4 shows the tip current under the tunneling condition, obtained on a Ge island (Fig. 4, right) under drift-free conditions. The tip current was measured in the constant-height mode to prevent a change in tunneling gap, where the feedback frequency was decreased to a value ten times lower than in the scanning mode. This profile shows a clear gap (32 pA) between 11.13 and 11.09 keV across the Ge absorption edge. The discrete jumps in current observed around 11.11 keV are simply due to discrete and periodic changes in the monochromator condition that is scanned step by step during the continuous tip-current measurement. This effect is inevitably stressed at points such as the absorption edge, at which the net signal intensity changes abruptly.

When the tip was retracted by about 400 nm from the surface, the current gap across the Ge absorption edge was 15 pA, which was independent of the position at the surface. Since the signal in this case is obviously composed of solely emitted electrons, this indicates that the above current gap of 32 pA under the tunneling condition contains a component (17 pA) that is different from the electrons collected from a wide area. Thus, the tunneling component is expected to have an improved spatial resolution. The clear current gap encourages attempting elemental analysis by comparing the values of the current gaps between different areas on the surface.

Profile (*b*) in Fig. 4 was obtained in the same manner as profile (*a*) for the surrounding area of the Ge island shown in Fig. 4 (right). The current gap at the Ge absorption edge is still observed in the surrounding area, in which the Ge concentration would be less than that in the Ge island. This suggests that the signal might contain many secondary electrons coming from the Ge atoms around the probe tip. However, the current gap is 40 pA, which is 8 pA larger than that for profile (*a*). This increase in current gap is not negligible, because the difference of 8 pA is approximately half of the above-mentioned increase in current (17 pA) from the tip-retracted condition (15 pA) to that of profile (*a*) (32 pA, tunneling condition on the Ge island). The latter increase (17 pA) was a current component expected to contain local information owing to the tunneling condition.

The difference in the current gap must appear in the higher-energy range because it is derived from the excitation of Ge atoms. The reason for the result obtained is that the incident energy was scanned from the higher to lower direction because of the monochromator specifications, and the total tip current was set commonly at the highest photon energy.

Since the drift-free condition was strictly maintained with atomic order, the modification of the current gap, which was reproducible, cannot be related to the shift of the probe tip. In addition, the emitted electrons cannot explain the increase in current gap on the surrounding area. This is because the emitted electrons must decrease the current gap on the surrounding area, in which the Ge atoms might be less concentrated than in the Ge island.

Fig. 5 shows the topographic (left) and scanned tip-current images (right) and their dependence on the incident photon energy (50 nm × 50 nm, −2 V, 0.5 nA for all images). The beam-induced tip-current image (right) was obtained simultaneously with the topographic image (left), and the images at different incident photon energies were compared across the Ge absorption edge. The tip-current image at higher photon energy shows the Ge island to be darker than the surrounding area, corresponding to the fact that the current gap decreases on the Ge island (Fig. 4). The averaged tip current in this image was 83 pA inside the Ge island, whereas it was 93 pA outside of the island, close to the values shown in Fig. 4 at high energy range. The difference of 10 pA between them is in good agreement with the difference of 8 pA in the current gap (Fig. 4). The decrease in the tip current on the Ge island was not observed at lower photon energy (Fig. 5*b*, right), which also indicates that the dark Ge island is not an effect of the modulated tunneling gap during the scan.

Our results suggest that the tip current can differ between the Ge island and the surrounding area, with a spatial resolution of at least the order of 10 nm. For determining more precise values of the spatial resolution, more detailed analysis is necessary, which is under progress.

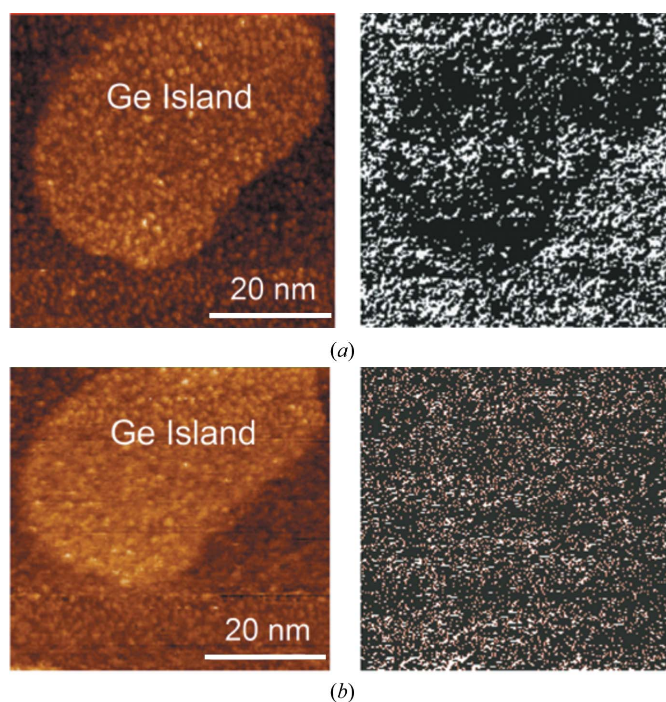

Figure 5
Energy dependence of the scanned image of the tip current (50 nm × 50 nm, −2 V, 0.5 nA for all figures). Topographic (left) and beam-induced tip-current images (right) were simultaneously obtained at higher [(*a*), 11.114 keV] and lower [(*b*), 11.090 keV] energies than the Ge absorption edge shown in Fig. 4.

4. Conclusions

In conclusion, a new synchrotron-radiation-based STM (SR-STM) system has been developed which enables *in situ* experiments with a hard-X-ray microbeam. By measuring the Ge nano-islands on a clean Si(111) surface, a modulation of the tip current was detected across the Ge absorption edge. The current gap across the Ge absorption edge was found to be different between the inside and outside of the Ge island. This result provides the possibility of elemental analysis of the order of 10 nm. Note that STM not only functions as an analytical tool but can also be used for manipulating atomic structures. The excitation of specific core electrons then appears attractive for deriving a selective reaction at nano-scale order on a surface, which is enabled by tuning the specific energy or polarization relating to the spin of synchrotron radiation. This is another advantage of SR-STM over other analytical methods based on a focused electron beam (Suenaga *et al.*, 2000) or synchrotron-radiation-based techniques that project emitted electrons (Schmidt *et al.*, 1998). The results presented in this report will allow us to investigate the chemical analysis or control the local reaction with the spatial resolution of STM.

We thank Dr K. Kobayashi (SPring-8), Professors Y. Taguchi (Osaka Prefecture University) and T. Sekitani (Hiroshima University) for discussions, and K. Tamasaku, Y. Nishino, Y. Yoda (SPring-8), SPring-8 staff, Mr S. Hirotsune (Hiroshima University) and Y. Ogawa (Osaka University) for experimental support. AS thanks Dr Y. Suzuki (SPring-8) for discussions. We thank Drs H. Takada, K. Suzuki and S. Kitamura (Jeol) for technical support. This study was supported in part by a Grant-in-Aid for Scientific Research (No. 14702021) from the Ministry of Education, Culture, Sports, Science and Technology.

References

Downes, A. & Welland, M. E. (1998). *Phys. Rev. Lett.* **81**, 1857–1860.
Grafström, S. (2002). *J. Appl. Phys.* **91**, 1717–1753.
Hasegawa, Y., Jia, J. F., Inoue, K., Sakai, A. & Sakurai, T. (1997). *Surf. Sci.* **386**, 328–334.
Hasegawa, Y., Tsuji, K., Nakayama, K., Wagatsuma, K. & Sakurai, T. (2000). *J. Vac. Sci. Technol. B*, **18**, 2676–2680.
Ishii, M. (2002). *Phys. Rev. B*, **65**, 85310.
Masuda, K. & Shigeta, Y. (2001). *Appl. Surf. Sci.* **175–176**, 77–82.
Matsushima, T., Okuda, T., Eguchi, T., Ono, M., Harasawa, A., Wakita, T., Kataoka, A., Hamada, M., Kamoshida, A., Hasegawa, Y. & Kinoshita, T. (2004). *Rev. Sci. Instrum.* **75**, 2149–2153.
Motta, N., Sgarlata, A., Calarco. R., Nguyen, Q., Patella, F., Castro Cal, J., Balzarotti, A. & De Crescenzi, (1998). *Surf. Sci.* **406**, 254–263.
Papanikolaou, N., Nonas, B., Heinze, S., Zeller, R. & Dederichs, P. H. (2000). *Phys. Rev. B*, **62**, 11118–11125.
Saito, A., Kuwahara, Y. & Aono, M. (2000). *4th International Workshop on the Use of Coherent Soft X-rays from a 27 m Long Undulator at SPring-8*, Hyogo, Japan, pp. 129.
Saito, A., Maruyama, J., Manabe, K., Kitamoto, K., Takahashi, K., Takagi, Y., Takami, K., Hirotsune, S., Tanaka, Y., Miwa, D., Yabashi, M., Ishii, M., Akai-Kasaya, M., Shin, S., Ishikawa, T., Kuwahara, Y. & Aono, M. (2006). *Jpn. J. Appl. Phys.* In the press.
Schmid, M., Stadler, H. & Varga, P. (1993). *Phys. Rev. Lett.* **70**, 1441–1444.
Schmidt, Th., Heun, S., Slezak, J., Diaz, J., Prince, K. C., Lilienkamp, G. & Bauer, E. (1998). *Surf. Rev. Lett.* **5**, 1287–1296.
Stipe, B. C., Rezaei, M. A. & Ho, W. (1998). *Science*, **280**, 1732–1735.
Suenaga, K., Tence, M., Mory, C., Colliex, C., Kato, H., Okazaki, T., Shinohara, H., Hirahara, K., Bandow, S. & Iijima, S. (2000). *Science*, **290**, 2280–2282.
Suzuki, S., Koike, Y., Fujikawa, K., Chun, W. J., Nomura, M. & Asakura, K. (2004). *Chem. Lett.* **33**, 636–637.
Takada, K., Takeuchi, M. & Takahashi, T. (2002). *Jpn. J. Appl. Phys.* **41**, 4990–4993.
Tsuji, K., Wagatsuma, K., Sugiyama, K., Hiraga, K. & Waseda, Y. (1999). *Surf. Interf. Anal.* **27**, 132–135.
Viernow, J., Petrovykh, D. Y., Kirakosian, A., Lin, J.-L., Men, F. K., Henzler, M. & Himpsel, F. J. (1999). *Phys. Rev. B*, **59**, 10356–10361.
Yabashi, M., Mochizuki, T., Yamazaki, H., Goto, S., Ohashi, H., Takeshita, K., Ohata, T., Matsushita, T., Tamasaku, K., Tanaka, Y. & Ishikawa, T. (2001). *Nucl. Instrum. Methods A*, **467–468**, 678–681.